# Joint Communications and Sensing Using Millimeter Wave Networks: A Bonus SAR

Husheng Li
The University of Tennessee, Knoxville, TN, USA
hli31@utk.edu

***Abstract*—In modern cellular communication networks, higher density of base stations and higher frequency bands will be employed. If being reflected by targets in the environment, the scattered communication signal also brings back the information of the targets, in addition to the communication messages, to the receivers. In this paper, it is proposed to leverage the reflected communication signals to reconstruct the image of the illuminated region. Due to the analogy to traditional synthetic aperture radar (SAR), the principle of spotlight SAR, namely the tomography via Fourier transformation, is adopted with necessary improvements. Numerical simulations are carried out to demonstrate the proposed algorithms.**

## I. Introduction

5G wireless communication networks have recently resulted in paradigm shift in industry and academia [1]. Motivated by the progress of 5G networks, the 6G networks are provisioned by researchers and industry. For simplicity, the 5G and beyond networks are called the 5G+ networks (a.k.a. NextG networks). A common knowledge in the community of wireless communications is that the environment causes substantial impact on communication signals. For example, the reflection of communication signals at various reflectors will substantially attenuate the signal strength, thus degrading the signal-to-noise ratio (SNR). In particular, for higher data transmission rate and ultra-short delay, the 5G+ networks expect to use higher frequency bands, such as the millimeter wave (mmWave) and TeraHz bands. These high frequency bands are even more susceptible to the environment, such as rain fade [15] and blockage [8]. However, despite being bad news to communications, the sensitivity of communication signals to the environment could benefit the task of sensing, as the other side of the same coin, since the environment information is embedded in the impact on communication signals. Therefore, the negative impact of environment on 5G+ communication signals can be leveraged to sense the environment, thus being a blessed misfortune. From an alternative perspective, sensing needs illuminations. Then, the communication signal in 5G+ networks can serve as the illumination, as a spotlight using invisible EM waves.

In this paper, we study the outdoor environment sensing using communication signals. This communication-network-based imaging is expected to work as follows: as illustrated in Fig. 1, a base station sends out communication signals (e.g., a broadcast of system information), which are reflected in the environment and received by other base stations (only one is illustrated in the figure); the transmitted and received signals are both sent to a processing center in the network to reconstruct the image (or more precisely, the scattering coefficient) of the illuminated area. We consider only the base stations for signal transmission and reception, as well as the core network for data processing in this imaging procedure, since the precise positioning and measurement feedback of user equipments (UEs) are difficult. The environmental imaging will find many applications after image analysis and understanding (which is beyond the scope of this paper), such as detecting speeding vehicles (by identifying moving reflectors) and monitoring flooding (by detecting water-like reflectors). Moreover, the sensing function is transparent to the communications, thus causing negligible impairment on the data transmissions. One traditional sensing facility is the synthetic aperture radar (SAR), which uses multiple virtual receivers formed by a mobile transceiver to collect the data and reconstruct the image of the illuminated region. In this paper, we will adopt the principle of SAR, with substantial revisions, due to the difference that SAR is mobile while communication networks considered in this paper are fixed (thus causing the sparsity of baselines and the bi-static sensing setups), and 5G+ communications use OFDM signaling, instead of pulses. Essentially, we will develop a Fourier transform framework to bridge the source and the field, such that the image can be obtained from an inverse transform.

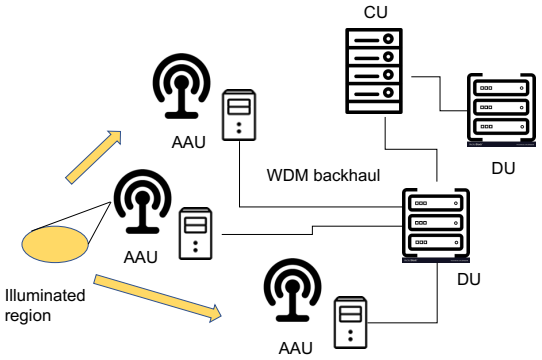


Fig. 1: A possible network architecture for 5G+ communication based sensing.

The remainder of this paper is organized as follows. In Section II, the related works and the principle of SAR are briefly introduced. The system model is explained in Section III. Then, the SAR-like imaging algorithms are detailed in Section IV. The system performance is analyzed theoretically and numerically in Section V. The final conclusions are given in Section VI.

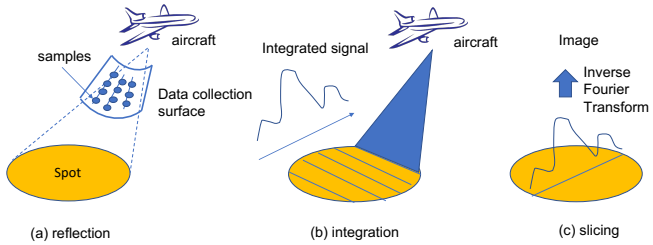


Fig. 2: An illustration of spotlight SAR.

## II. Related Work

In this section, we introduce the related works, including sensing schemes using communication signals and the principle of spotlight SAR.

### A. Communication Signal for Sensing

There have been substantial studies on leveraging communication signals for imaging [16], [17], particularly in the mmWave band. In a contrast, these studies are mainly focused on indoor imaging for the purpose of inferring locations and surface properties of targets, based on monostatic transceivers, while our proposed network-wide sensing is mainly for *outdoor* imaging using wide-area cellular network. Moreover, in [16], [17] only the information of RSS and angle of arrival (AOA) are used, which limits the imaging of targets having strong directionality of reflections. In [**?**], full-duplex Qualcomm IEEE 802.11ad/ay chipsets in the 60GHz band are used for multi-person locationing by leveraging periodic pulses and beamforming. The corresponding imaging is based on estimating the silhouette by radar ranging, instead of estimating the scattering coefficients of the target. So are the studies in [2], [10]. The studies on OFDM signal based passive radar [**?**], [3] are closer to our proposed imaging scheme, since both consider wide-band OFDM signals used in 4G and 5G cellular systems. However, these studies detect only significant scatterers; e.g., in the experiment of [**?**], only a few artificially placed reflectors are located.

### B. Principle of Spotlight SAR

Beam-scanning SAR is based on the sensing along the range and azimuth directions, using round trip time estimation and Doppler estimation [4]. It relies on the motion of the radar platform, thus being unsuitable to the fixed communication-network-based sensing. Therefore we focus on the spotlight SAR imaging [6], which is based on that of tomography, namely the celebrated projection-slice theorem. Take a 2-dimensional target, whose support region is $\Omega$, for instance. The pixels (say, the reflectivity of the surface) are given by $g(x, y)$, $(x, y) \in \Omega$. Then, the corresponding 2-dimensional Fourier transform is given by

$$G(jX, jY) = \int_{\Omega} g(x, y) e^{-j(xX+yY)} dxdy. \tag{1}$$

Consider the image resulting from the projection of $g(x, y)$ on a line, say the $y$-axis. The integrated signal on the $y$-axis is given by $h(y) = \int_{\Omega} g(x, y)dx$, whose Fourier transform is denoted by $H(jY) = \int_{\Omega} h(y)e^{-jyY} dy$. Then, the projection-slice theorem states that the Fourier transform $H(jY)$ equals the values of $G(jX, jY)$ on the line passing the origin and being parallel to the $y$-axis, namely $H(jY) = G(0, jY)$.

Based on the projection-slice theorem, the mechanism of spotlight SAR imaging is illustrated in Fig. 2. The aircraft illuminates the given region by sending out radar pulses, as in Fig. 2 (a). Then, the radar signal reflected by the targets on the line orthogonal to the illuminating beam (as shown in Fig. 2 (b)) arrives at the radar receiver simultaneously, thus resulting in the integral of the reflectivities on the line. By leveraging the arrival times of reflected radar signals, the radar receiver can obtain the integrated signal on each orthogonal direction. According to the projection-slice theorem, the radar receiver can attain the slice of 2-dimensional Fourier transform $G$ of the reflectivities in the illuminated region, by fitting the spectrum $H$ of the integrated signal to the origin. If the aircraft changes multiple directions, it obtains the values of the 2-dimensional Fourier transform along multiple slicing lines passing the original. When sufficiently many slices have been obtained, the reflectivities of the illuminated region, namely the image, can be obtained from inverse Fourier transform, as shown in Fig. 2 (c). *Note that, in the spotlight SAR, the transmitter and receiver are located at the same position, which is not true in the communication network. Moreover, OFDM signaling is used in 5G+ communications, instead of the pulses used in SAR. Therefore, substantial revisions are needed for the proposed sensing scheme.*

## III. System Model

We assume that there are totally $N$ base stations within a certain area, with perfect time synchronization[1]. Each could be transmitting or receiving. When transmitting data, a base station uses a frequency band with $M$ subcarriers, with initial frequency $f_c$ and frequency step $\delta f$. Each base station is equipped with $N_a$ antennas. The height of each base station is assumed to be perfectly known. We consider 2-dimensional reflections of transmitted signal on the ground. The reflectivity (or scattering coefficient) at position $(x, y)$ is a complex number, which can be written as $g(x, y) = |g(x, y)|e^{j\phi(x,y)}$. Note that the imaginary part of the reflectivity stems from random phase change at the reflectors. In practice, the phase part $e^{j\phi(x,y)}$ changes much more radically than the magnitude $|g(x, y)|$. It is assumed that the base stations send their raw measurements to a data processing center for imaging the illuminated regions. A possible network architecture is illustrated in Fig. 1: the active antenna units (AAUs) transmit or receive radio frequency (RF) signals, while the measurements can be collected at the distributed units (DUs) and further centralized units (CUs), via WDM optical fibers, for further data processing.

## IV. Spotlight-SAR-Like Imaging

In this section, we propose an imaging algorithm using multiple base stations and the principle of spotlight SAR (introduced in Section II). However, the principle cannot be employed directly, due to the different positions of transmitter

[1]In practice, the time synchronization of base stations can be achieved by using GPS, calibration signals, or autofocusing techniques.

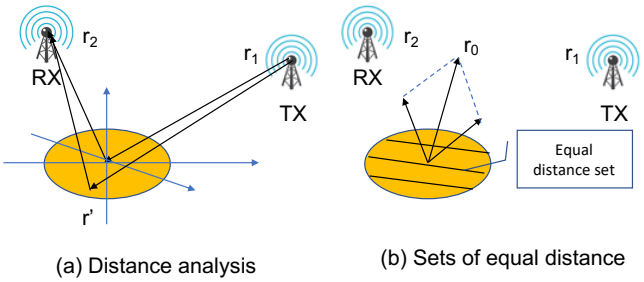


Fig. 3: Calculation of distance.

and receiver in the communication network (similarly to multi-static radar). As will be seen, the imaging procedure can be modified to fit the context of communication-network-based sensing, by following the principle of slicing and interpolation.

### A. Slicing

Following the principle of spotlight SAR, our first step is to estimate the spectrum slices of the illuminated area. For simplicity, we assume that the origin is located within the illuminated area. Consider a point $\mathbf{r}'$ in the illuminated area. Assume that the positions of the transmitter and receiver are $\mathbf{r}_1$ and $\mathbf{r}_2$, respectively. The distance from an illuminated point $\mathbf{r}'$ to the transmitter is given by

$$\|\mathbf{r}' - \mathbf{r}_1\| \approx \|\mathbf{r}_1\| + \mathbf{r}' \cdot \frac{\mathbf{r}_1}{\|\mathbf{r}_1\|}, \tag{2}$$

where the approximation is valid when $\|\mathbf{r}_1\| \gg \|\mathbf{r}'\|$. We have a similar conclusion for $\|\mathbf{r}' - \mathbf{r}_2\|$.

Therefore the traveling distance of the signal sent from the transmitter at $\mathbf{r}_1$, reflected at $\mathbf{r}'$, and received by the receiver at $\mathbf{r}_2$, is approximated by

$$\begin{aligned} & \|\mathbf{r}' - \mathbf{r}_1\| + \|\mathbf{r}' - \mathbf{r}_2\| \\ \approx \quad & \|\mathbf{r}_1\| + \|\mathbf{r}_2\| + \mathbf{r}' \cdot \left( \frac{\mathbf{r}_1}{\|\mathbf{r}_1\|} + \frac{\mathbf{r}_2}{\|\mathbf{r}_2\|} \right). \end{aligned} \tag{3}$$

Hence, the set of reflection points that result in the same traveling time is given by

$$\mathbf{r}' \cdot \left( \frac{\mathbf{r}_1}{\|\mathbf{r}_1\|} + \frac{\mathbf{r}_2}{\|\mathbf{r}_2\|} \right) = \text{constant}, \tag{4}$$

which is an approximately the straight line perpendicular to the direction

$$\mathbf{r}_0 = \frac{\mathbf{r}_1}{\|\mathbf{r}_1\|} + \frac{\mathbf{r}_2}{\|\mathbf{r}_2\|}, \tag{5}$$

as illustrated in Fig. 3 (b). Hence, a measurement at the receiver collects the integrated signals from the equal distance lines.

### B. Impulsive Response

When the signal sent from the transmitter is a delta function $\delta(t)$, the received signal is exactly the accumulated signal $h(t)$ along the direction specified by $\mathbf{r}_0$, namely

$$h(t) \propto \int_{\|\mathbf{r}_1\| + \|\mathbf{r}_2\| + \mathbf{r}' \cdot \mathbf{r}_0 = ct} g(\mathbf{r}') d\mathbf{r}', \tag{6}$$

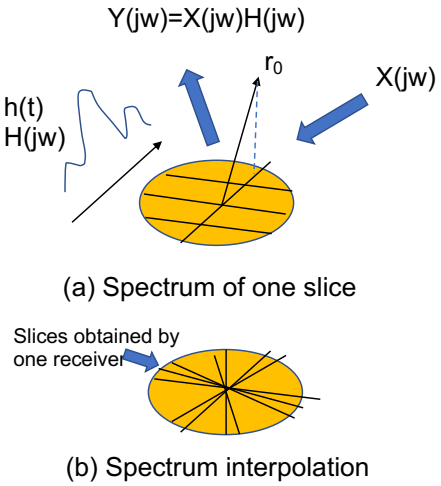


Fig. 4: Slicing and interpolation in the spectrum.

which is the accumulated reflectivity along the equal distance line (recall that $g$ is the reflectivity of the illuminated point). The profile of $h(t)$ can be used to reconstruct the slice of Fourier transform of the charge density of the illuminated region, by leveraging the projection-slice theorem. However, different from SAR systems, the communication systems do not use pulse waveforms, which can obtain $h(t)$ directly (e.g., sampling the reflected pulses). Therefore, we consider the subsequent two approaches that are essentially equivalent but take different paths to the desired result.

*1) Spatial Fourier Transform:* We first notice that the impulse response $h(t)$ is indeed also a function of space, which can be written as $h(r)$ (without changing the notation for simplicity), where $r = ct$ is the EM wave propagation distance. Therefore, we can consider $h(r)$ as a virtual source charge distribution, supported within $(-r_m, r_m)$, where $2\delta r$ is the range of the propagation distance and the distance between the source center and the receiver is $d$. Given a single-tone carrier input with wavenumber $k = \frac{1}{\lambda}$ and without modulation, the received signal is given by

$$\begin{aligned} H(t,k) &= \int_{-r_m}^{r_m} h(r) e^{-j((r+d)k + wt)} dr \\ &= e^{-jwt} e^{-jdk} \int_{-r_m}^{r_m} h(r) e^{-jrk} dr. \end{aligned} \tag{7}$$

By demodulation (to remove $e^{-jwt}$) and phase alignment (to remove $e^{-jdk}$), we obtain the complex scalar:

$$H(k) = \int_{-r_m}^{r_m} h(r) e^{-jrk} dr, \tag{8}$$

which shows that the received signal $H(k)$ is the spatial Fourier transform of $h(r)$. Notice that $H(k)$ is simply the received signal at the corresponding subcarrier with frequency $ck$. Therefore, we use the received signals $\{H_m\}_{m=1,\ldots,M}$ on the different subcarriers as the samples of $H(k)$ in the wavenumber space, as the samples in the spatial spectrum of the reflectivity of the illuminated area. Then, the samples $\{H_m\}_{m=1,\ldots,M}$ can be applied to the projection-slice theorem for the final image reconstruction.

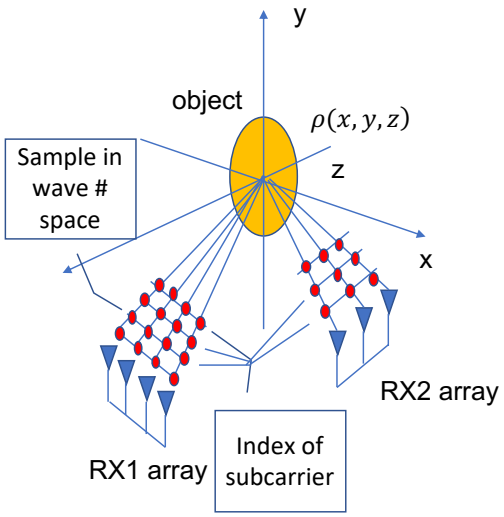


Fig. 5: Sampling in the wave number space.

*2) Frequency Response:* We can also consider the illumination procedure as a linear system, where $h(t)$ is the impulse response, while the input and output are the transmitted and received signals. The transfer function $H(jw)$ equals the Fourier transform of $h(t)$. In practice, the transmitted signal cannot be an impulse $\delta(t)$. When the spectra of the transmitted and received signals are $X(jw)$ and $Y(jw)$, respectively, the transfer function $H$ can be estimated as $H(jw) = \frac{Y(jw)}{X(jw)}$. When OFDM is employed, we obtain the sample estimations of the transfer function:

$$H(jw_m) = \frac{Y_m}{X_m}, \qquad m = 1, ..., M, \tag{9}$$

where $w_m$ is the frequency of the $m$-th subcarrier, $Y_m$ and $X_m$ are the received and transmitted signals on the $m$-th subcarrier, respectively. This is illustrated in Fig. 4 (a). Notice that $H(jw_m)$ is simply $H_m$ in the above discussion. Therefore, the two approaches are essentially the same.

### C. Data Collection Surface

Since we assume multiple receive antennas at each receiver, each antenna represents a slice of the Fourier transform domain of the reflectivity in the illuminated area. When the antenna arrays are linear, the data can be intuitively represented by data collection surfaces, illustrated in Fig. 5, where the two data collection surfaces of two different receiving base stations are shown. The cross side of the surface is the direction of the antennas, while the range side means the wave number dimension. We denote by $H^n_{ml}$ the spatial-spectrum data on the $l$-th subcarrier at the $m$-th antenna of the $n$-th base station. The data forms a grid on the data collection surface. We denote by $X$ the cross axis and $Y$ the ranging axis. Therefore, the data can be denoted by $H^n(X_l, Y_m)$.

### D. Reconstruction by IDFT and Fusing

In the above inversion algorithm, a large matrix needs to be inversed, which results in substantial computational cost. In traditional SAR systems, the spatial samples in the image can be easily computed using IDFT, since the measurements collected in the data patches are the Fourier transform of the image. Although the data patch is only a portion of the spatial spectrum, the spectrum center can be shifted to the center of the patch for IDFT. Different from the traditional SAR system in which there is only one data patch, we are facing multiple isolated data patches in the communication network based imaging. Therefore, in this paper, we propose IDFT-based inversion and fusion for the distinct patches. For each data patch, we rotate the orientation to the direction $\mathbf{r}_0$, and shift the center of the spatial spectrum to that of the data patch. The spatial spectrum is normalized by the offset of the minimum of $\mathbf{k} \cdot \mathbf{r}$, which is for the application of DFT:

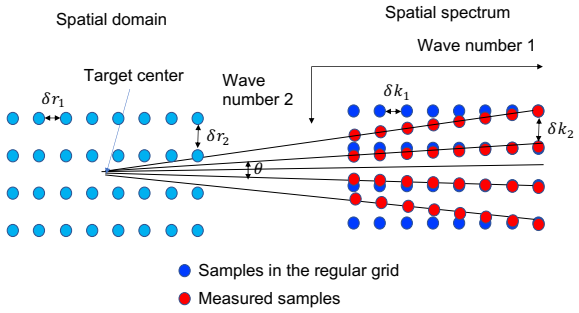


Fig. 6: The setup of 2-dimensional DFT and IDFT.

$$\bar{H}^n_{lm} = \bar{H}^n_{lm} e^{j \min_{\mathbf{r}}(\mathbf{k}\cdot\mathbf{r})}. \tag{10}$$

After the shift of center, the spatial spectrum at base station $n$ sampled at the grid $\{m\delta k_1, n\delta k_2\}_{m=1,...,M,n=1,...,N_a}$, is given by

$$\begin{aligned} \bar{H}^n_{lm} &\propto \int g(\mathbf{r}) e^{-i\mathbf{k}_{lm}\cdot\mathbf{r}} d\mathbf{r} \\ &\approx \sum_{a,b} g_{a,b} e^{-i(al\delta k_1 \delta r_1 + bm\delta k_2 \delta r_2)} \\ &= \sum_{a,b} g_{a,b} e^{-i\left(\frac{al}{M} + \frac{bm}{N_a}\right)}, \end{aligned} \tag{11}$$

where the step parameters $\delta k_1$, $\delta k_2$, $\delta r_1$ and $\delta k_2$ are chosen such that $M = \frac{1}{\delta k_1 \delta r_1}$ and $N_a = \frac{1}{\delta k_2 \delta r_2}$, in order for the 2-dimensional inverse DFT.

We select the following parameters $\delta k_1$, $\delta k_2$, $\delta r_1$ and $\delta k_2$:

- We select $\delta k_1$ and $\delta k_2$ such that the samples at $\{m\delta k_1, n\delta k_2\}_{m=1,...,M,n=1,...,N_a}$ are close to the measured samples $\tilde{H}_{mn}$:

$$\begin{cases} \delta k_1 = \frac{\delta f}{c} \cos\left(\frac{\theta}{2}\right) \\ \delta k_2 = \frac{\delta f}{c} \sin\left(\frac{\theta}{2}\right) \end{cases}. \tag{12}$$

- We select $\delta r_1$ and $\delta r_2$ as

$$\begin{cases} \delta r_1 = \frac{1}{M\delta k_1} \\ \delta r_2 = \frac{1}{N_a \delta k_2} \end{cases}. \tag{13}$$

The spatial spectrum samples $\{\bar{H}^n_{lm}\}_{lm}$ are obtained from the interpolations of the measured samples $\{\tilde{H}^n_{lm}\}_{lm}$. Then, the spatial samples of the images at positions $\{a\delta r_1, b\delta r_2\}$ are obtained from the inverse DFT of the spatial spectrum samples at $\{\bar{H}^n_{lm}\}_{lm}$. Once the reconstructed images of the same illuminated area have been obtained from distinct data patches, we can fuse them into the same image by interpolating among

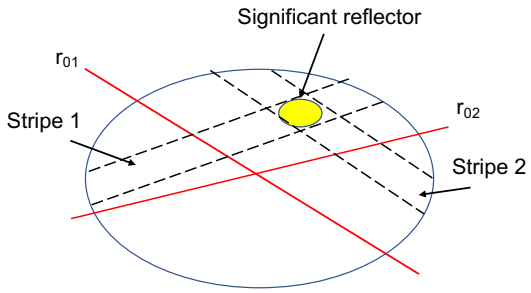


Fig. 7: Estimation of significant reflector with the lack of cross resolution.

the reconstructed samples. The procedure is summarized in Procedure 1.

**Algorithm 1**

1: **for** Each receiving BS **do**
2: Calibrate the received signals.
3: Rotate the orientation and shift the center.
4: Determine the parameters $\delta k_1$, $\delta k_2$, $\delta r_1$ and $\delta r_2$ using (12) and (13).
5: Carry out interpolation for the spatial spectrum samples at regular grid.
6: Carry out IDFT to obtain the spatial image.
7: **end for**
8: Carry out interpolation using the reconstructed images.

### *E. Reconstruction with Insufficient Cross Resolution*

A major challenge to the communication-network-based imaging is the cross direction resolution. In traditional SARs, the cross resolution is assured by the long flight trajectory of aircraft. However, in the proposed communication-network-based imaging, for each base station, the cross direction span is determined by the size of antenna array. When the antenna spacing is $\frac{\lambda}{2}$, the cross direction resolution is $\delta x \approx \frac{\lambda}{2N_a\frac{\lambda}{2d}} = \frac{d}{N_a}$, which equals 1.56m when $d = 100m$ and $N_a = 64$. The resolution becomes even worse when $N_a$ is small. In such a scenario, only the range direction information (range and width) is obtained from the Fourier transform. When there are two base stations receiving the signal, we can use the intersection of the perpendicular lines to locate the significant reflector, as illustrated in Fig. 7.

## V. Imaging Error Evaluation

In this section, we analyze the error of imaging using both theoretical and numerical approaches.

### *A. Theoretical Analysis*

For the error analysis of imaging, we assume a large number of base stations and model the sidelobe cancellation effect using a random process. We obtain the following expression of the MSE, which decreases inversely proportional to $N$, when $N$ is sufficiently large.

**Theorem 1.** *For sufficiently large $N$, the MSE of image reconstruction is given by*

$$\begin{aligned} & E[|g(x)-\hat{g}(x)|^2] \qquad (14)\\ = \; & \frac{1}{2N^3}|g(x)|^2\sum_{t\neq 0}\text{sinc}^2(t)+\frac{1}{N}\sum_{t\neq x}|g(t)|^2\text{sinc}^2(x-t), \end{aligned}$$

*Proof.* We define $s(x) = \sum_{n=1}^{N} e^{-jxX_n}$. We then calculate the autocorrelation of $s(x)$, where $\delta x \neq 0$:

$$\begin{aligned} & E[s(x)s^*(x+\delta x)]\\ = \; & E\left[\sum_{n=1}^{N} e^{-jxX_n}\sum_{m=1}^{N} e^{jxX_m}\right]\\ = \; & \sum_{n=1}^{N} E\left[e^{j\delta x X_n}\right]+\sum_{n\neq m} E\left[e^{-j(xX_n-xX_m-\delta x X_m)}\right]\\ = \; & \sum_{n\neq m} E\left[e^{-jxX_n}\right]E\left[e^{-j(x+\delta x)X_m}\right]=0, \qquad (15) \end{aligned}$$

where the third equality is due to the fact $E\left[e^{j\delta x X_n}\right]$, and factorization in the fourth equality is due to the independence of $\{X_n\}_{n=1,\ldots,N}$. Therefore, we can model $s(x)$ as an i.i.d. Gaussian random sequence with variance $\frac{1}{N}$, except for $s(0) = N$.

The reconstruction of the image is then given by the following output of linear system: $\hat{g}(x) = (g * h)(x)$, where the impulse response $h$ is given by $h(x) = \frac{s(x)\text{sinc}(x)}{\sqrt{\sum_x |s(x)|^2\text{sinc}^2(x)}}$. Here the denominator is to normalize energy of $h(x)$. Due to the law of large numbers, we have $h(0) \approx 1-\frac{1}{2N^3}\sum_{t\neq 0}\text{sinc}^2(t)$. We consider the MSE of the estimated complex reflectivity, which is given by

$$\begin{aligned} E[|g(x)-\hat{g}(x)|^2] &= E[|g*\delta(x)-g*h(x)|^2]\\ &= E[|g*\Delta h(x)|^2], \qquad (16) \end{aligned}$$

where $\delta$ is the discrete time delta function and $\delta h$ is the difference between $\Delta$ and $h$. Then, we further have

$$\begin{aligned} & E[|g(x)-\hat{g}(x)|^2]\\ = \; & E\left[\sum_t g(t)\Delta h(x-t)\sum_s g^*(s)\Delta h^*(x-s)\right]\\ = \; & E\left[\sum_t |g(t)|^2|\Delta h(x-t)|^2\right]\\ = \; & |g(x)|^2|\Delta h(0)|^2+\sum_{t\neq 0}|g(t)|^2E[|\Delta h(x-t)|^2], \qquad (17) \end{aligned}$$

which leads to the conclusion. □

### *B. Numerical Results*

We consider a region, in which the base stations are located on a regular grid with spacing of 200m. In each time slot, each base station sends out a beam which is modeled as a cone. We randomly place 30 significant reflectors in a 800m×800m square region, each being a 10m×10m square. The background is dark. We consider 256 subcarriers and the total bandwidth of signal is 512MHz, in the band of 5GHz. The open angle of beam is 5 degrees. At each time slot, the probability for each base station to transmit is 0.05, which randomly selects one of 5 channels to transmit, while the receivers also randomly select the channels. We further

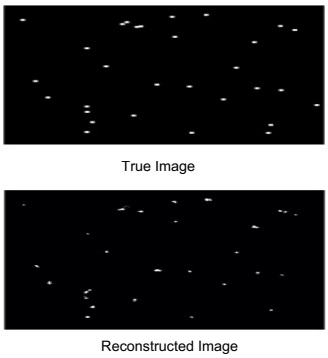


Fig. 8: Target reconstruction: true and estimated.

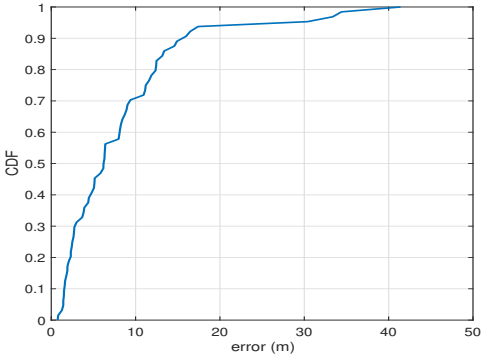


Fig. 9: CDF of absolute error of target center estimation.

assume that only base stations within 400 meters to the illuminated region receive the signal for further analysis, since a further distance will yield a substantially low signal power. For simplicity, we consider only the noise-free case, and will leave the impact of noise to the future research. This is reasonable since we assume a very small beam open angle, such that the power path loss is small. We also consider 64 antennas at each base stations, with the spacing of half carrier wavelength. Therefore, we can only obtain a reasonable resolution in the radius direction. Hence, we use the fusion algorithm in Section IV-E. The comparison between the original image and the reconstructed image (after 2000 time slots) are given in Figure 8 for one realization. We observe that most of the significant reflectors have been identified, while there are also some false detections. The absolute error cumulative distribution function (CDF) of target center estimation is shown in Fig. 9, while the CDF of the estimated target radius is given in Fig. 10 (the correct value is $5\sqrt{2}$m); both are obtained from 100 realizations of targets. We observe that the errors are reasonable; but refinements are needed for future research.

## VI. Conclusion

In this paper, we have studied the imaging of outdoor environment using communication signals and infrastructure. The imaging principle of SAR is leveraged for the communication-signal-based imaging, by addressing the difference of the scenarios. The framework of Fourier transform is employed for the image reconstruction. Various challenges, such as

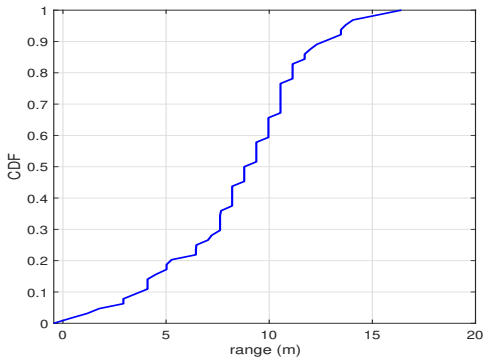


Fig. 10: CDF of target radius estimation.

multi-static signaling, OFDM waveform and distributed data patches, have been addressed. Numerical simulations have been carried out for the imaging of randomly distributed significant reflectors, which have demonstrated the validity of the proposed algorithms.

## References

[1] M. Agiwal, A. Roy, N. Saxena, "Next generation 5G wireless networks: A comprehensive survey," *IEEE Communications Surveys & Tutorials*, vol.18, no.3, pp.1617–1655, 2016.

[2] M. Aladsani, A. Alkhateeb and G. C. Trichopulos, "Leveraging mmWave Imaging and Communications for Simultaneous Localization and Mapping," in *Proc. of IEEE International Conference on Acoustics, Speech and Signal Processing (ICASSP)*, 2019.

[3] M. Braun, C. Sturm, and F. Jondral. "Maximum likelihood speed and distance estimation for OFDM radar." *Proceedings of the 2010 IEEE Radar Conference,* Washington, D.C., May 10—14, pp. 256—261, 2010.

[4] I. G. Cumming and F. H. Wong, *Digital Processing of Synthetic Aperture Radar Data: Algorithms and Implementation*, Artech House, 2002.

[5] A. J. Devaney, *Mathematical Foundations of Imaging, Tomography and Wavefield Inversion*, Cambridge University Press, 2012.

[6] C. V. Jakowatz, Jr, D. E. Wahl, P. H. Elchel, et al, *Spotlight-mode Synthetic Aperture Radar: A Signal Processing Approach*, Springer, 1999.

[7] D. C. Munson, Jr and J. L. C. Sanz, "Image reconstruction from frequency-offset Fourier data,", *Proc. of IEEE*, vol.72, no.6, pp. 661-669, June 1984.

[8] S. Singh, F. Ziliotto, U. Madhow, E. Belding, and M. Rodwell, "Blockage and directivity in 60 Ghz wireless personal area networks: From crosslayer model to multihop mac design," *IEEE Journal on Selected Areas in Communications*, vol. 27, no. 8, 2009.

[9] R. J. Sullivan, *Microwave Radar: Imaging and Advanced Concepts*, Artech House, 2000.

[10] C. Sturm, S. Schulteis and W. Wiesbeck, "Two-dimensional radar imaging with scattered PSK-modulated communication signals," in *Proc. of European Radar Conference*, 2007.

[11] R. J. Sullivan, *Microwave Radar: Imaging and Advanced Concepts*, Artech House, 2000.

[12] T. George and F. Ross, *Calculus and Analytic Geometry*, Addison-Wesley, 1979.

[13] A. Zangwill, *Modern Electrodynamcis*, Cambridge University Press, 2013.

[14] Z. Zhang and H. Li, "Sensing wind velocity by leveraging millimeter wave communications," *IEEE DySPAN Workshop,* 2019

[15] Q. Zhao and J. Li, "Rain attenuation in millimeter wave ranges," in *2006 7th International Symposium on Antennas, Propagation & EM Theory*, 2006.

[16] Y. Zhu, Y. Zhu, B. Zhao, and H. Zheng, "Reusing 60GHz radios for mobile radar imaging," in *Proc. of Annual International Conference on Mobile Computing and Networking (MobiCom)*, 2015.

[17] Y. Zhu, Y. Zhu, Y. Zhang, Z. Zhao, and H. ZHENG, "60GHz mobile imaging radar." in *Proc. of HotMobile*, 2015.